# Solution Structural Study of a DNA Duplex Containing the Guanine-N7 Adduct Formed by a Cytotoxic Platinum−Acridine Hybrid Agent[†,‡]

Hemanta Baruah, Marcus W. Wright, and Ulrich Bierbach*

*Department of Chemistry, Wake Forest University, P.O. Box 7486 Reynolda Station, Winston-Salem, North Carolina 27109*

*Received January 5, 2005; Revised Manuscript Received February 27, 2005*

ABSTRACT: [PtCl(en)(ACRAMTU-*S*)]$(NO_3)_2$ (PT-ACRAMTU; en = ethane-1,2-diamine, ACRAMTU = 1-[2-(acridin-9-ylamino)ethyl]-1,3-dimethylthiourea) is a dual metalating/intercalating DNA binding drug conjugate that shows cytotoxicity at micromolar to nanomolar concentrations in a wide range of solid tumor cell lines. In ∼80% of its adducts, PT-ACRAMTU binds to guanine-N7 in the major groove, selectively at 5′-CG sites [Budiman, M. E. et al. (2004) *Biochemistry 43*, 8560−8567]. Here, we report the synthesis, physical characterization, and NMR solution structure of a site-specifically modified octamer containing this adduct, 5′-CCTCG*TCC-3′/3′-GGAGCAGG-5′, where the asterisk indicates the [Pt(en)-ACRAMTU)]$^{3+}$ fragment. The structure was determined by a combination of high-resolution 2-D NMR spectroscopy and restrained molecular dynamics/molecular mechanics (rMD/MM) calculations using 179 NOE distance restraints and refined to an $r^6$ weighted residual ($R^x$) of $9.2 \times 10^{-2}$ using the complete relaxation matrix approach. An average structure was calculated from the final ensemble of 19 rMD geometries showing pairwise root-mean-square deviations of <1.05 Å. The dual binding increases the thermal stability of the octamer compared to the unmodified duplex ($\Delta T_m = 13.2°$). The modified sequence shows structural features reminiscent of both B- and A-type DNA. Watson−Crick hydrogen bonding is intact at and beyond the adduct site. Platinum is bound to the N7 position of G5 in the major groove, and ACRAMTU intercalates into the central 5′-C4G5/C12G13 base-pair step on the 5′-face of the platinated nucleobase. The chromophore's long axis is aligned with the long axes of the adjacent base pairs, maximizing intermolecular $\pi-\pi$ stacking interactions. PT-ACRAMTU lengthens (rise, 6.62 Å) and unwinds (twist, 15.4°) the duplex at the central base-pair step but does not cause helical bending. No C3′-*endo* deoxyribose pucker and no significant roll are observed at the site of intercalation/platination, which clearly distinguishes the PT-ACRAMTU-induced damage from the 1,2-intrastrand cross-link formed by cisplatin. Overall, the DNA perturbations produced by PT-ACRAMTU do not appear to mimic those caused by the major cisplatin lesion. Instead, intriguing structural similarities are observed for PT-ACRAMTU's monoadduct and the N7 adducts of dual major-groove alkylating/intercalating antitumor agents, such as the pluramycins.

Platinum−intercalator hybrid pharmacophores have been a major focus area in platinum antitumor chemistry for the past two decades (*1*). The design of these conjugates was aimed at improving the efficacy of clinically established agents, such as cisplatin[1] (Chart 1), by reducing the drug's residence time in the cytosol and enhancing its binding kinetics with nuclear DNA, the putative therapeutic target (*1*). It was also hoped that the combination of traditional agents in a single molecule would lead to additive or synergistic activity (*1*). In the majority of lesions produced in double-stranded DNA, cisplatin induces cross-links between adjacent purine bases of the same strand (1,2-intrastrand cross-links) (*2*). The formation of these bifunctional adducts, which involves platination of the N7 endocyclic nitrogens of guanine (G) and adenine (A) at GG and 5′-AG sites, occurs without long-range sequence specificity (*3*). The cytotoxic effect of cisplatin and other DNA damaging agents is mediated by enzymes and proteins that interact with the structurally altered DNA in a sequence- and/or groove-specific manner (*4*). A major goal in DNA-directed cancer chemotherapy, therefore, is to identify small molecules with enhanced sequence and groove read-out, which can be targeted more selectively to processes critical to cell proliferation (*4*). Thus, in addition to the pharmacokinetic advantages of the drug conjugates, the tethering of *cis*-platinum complexes to intercalators (*1*) and groove binders (*5*, *6*) was

[†] This research was supported by a grant from the National Cancer Institute, CA101880.

[‡] Atomic coordinate and distance restraints files for the refined structure have been deposited with the Brookhaven Protein Data Bank (PDB code 1XRW).

* To whom correspondence should be addressed. Tel: (336) 758−3507. Fax: (336) 758−4656. E-mail: bierbau@wfu.edu.

[1] Abbreviations: ACR, acridine; ACRAMTU, 1-[2-(acridin-9-ylamino)ethyl]-1,3-dimethylthiourea; CD, circular dichroism; cisplatin, *cis*-diamminedichloroplatinum(II), *cis*-$[PtCl_2(NH_3)_2]$; dGuo, 2′-deoxyguanosine; dqf-COSY, double quantum-filtered correlated spectroscopy; en = ethane-1,2-diamine; dsDNA, double-stranded DNA; G*, platinated guanine-N7; HMG, high-mobility group; HPLC, high-performance liquid chromatography; ICD, induced circular dichroism; MALDI-TOF, matrix-assisted laser desorption ionization time-of-flight; NOE, nuclear Overhauser effect; NOESY, nuclear Overhauser enhancement spectroscopy; PT-ACRAMTU, [PtCl(en)(ACRAMTU-*S*)]$(NO_3)_2$; rMD/MM, restrained molecular dynamics/molecular mechanics; RMSD, root-mean-square deviation; TOCSY, total correlation spectroscopy.

10.1021/bi050021b CCC: $30.25 
Published on Web 04/02/2005

Chart 1: Structures of Cisplatin, PT-ACRAMTU, the Major Mononucleoside Adduct Identified in Enzymatic Digests, dGuo*, and the Modified Duplex **III*** with Atom and Residue Numbering Scheme

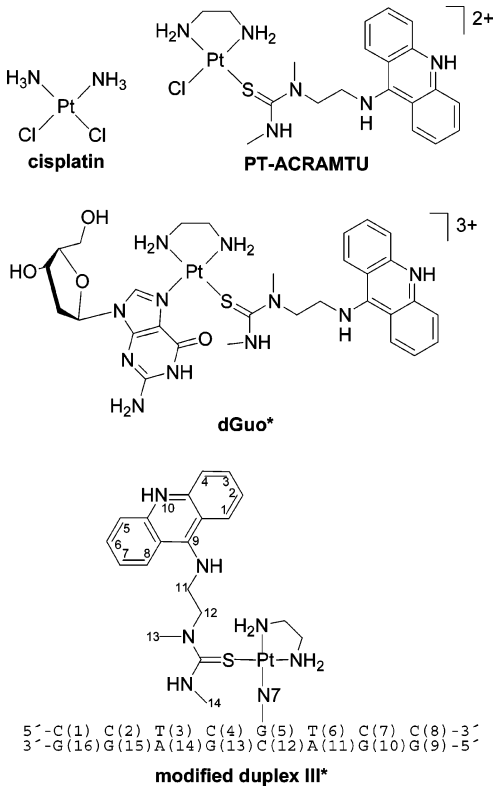


considered a viable strategy of tuning the DNA binding selectivity of the divalent metal. Unfortunately, in virtually all hybrid agents the metal moiety appears to dominate the DNA interactions leading to cross-link formation in runs of consecutive purines and adduct profiles similar to that of the parent platinum drug (*1*).

Recently, we have reported a novel non-crosslinking platinum−acridine pharmacophore (*7*) whose DNA interactions, unlike those of the "classical" conjugates, are clearly dominated by the nonleaving intercalating moiety. PT-ACRAMTU ([PtCl(en)(ACRAMTU-*S*)]$(NO_3)_2$, Chart 1; en = ethane-1,2-diamine, ACRAMTU = 1-[2-(acridin-9-ylamino)ethyl]-1,3-dimethylthiourea) is the prototype of a new class of cytotoxic agents displaying promising activity in a wide range of solid tumor cell lines (*7*−*9*). Previous biochemical and biophysical studies have shown that PT-ACRAMTU associates with dsDNA through a dual binding mode involving platinum binding to nucleobase nitrogen and intercalation of the acridine chromophore into the DNA base stack (*10*). The conjugate targets guanine (80%) and adenine (20%) bases (*11*) at the base-pair steps 5′-CG/CG, 5′-TA/TA, and 5′-GA/TC, which are the preferred intercalation sites of ACRAMTU, the platinum-free 9-aminoacridine derivative (*12*). The unique base-step recognition of PT-ACRAMTU ultimately leads to unprecedented monofunctional metalation of adenine in a minor fraction of adducts and a DNA adduct profile truly complementary to that of cisplatin and its derivatives. Using transcriptional footprinting and endonuclease cleavage assays, we found that the formation of the guanine adducts occurs selectively at 5′-CG sites but not at 5′-GC sites or in poly(G) tracts (*13*). As a consequence, PT-ACRAMTU and cisplatin produce guanine adducts at *mutually exclusive sites*. NMR and X-ray crystallographic data obtained for the major platinum-modified DNA fragment isolated from enzymatically degraded DNA, [Pt(en)(ACRAMTU)(dGuo)]$^{3+}$ (dGuo*, Chart 1), provided ultimate evidence for platinum binding to guanine-N7 (*14*).

To elucidate the structural impact of the guanine-N7 monoadduct of PT-ACRAMTU in dsDNA, we synthesized a site-specifically modified model duplex and characterized the adduct using a combination of thermal melting experiments and CD spectropolarimetry (*15*). In addition, molecular modeling techniques were applied to demonstrate that combined platination of G-N7 in the major groove and intercalation of the acridine moiety into the 5′-CG/CG base-pair step on the 5′-face of the modified purine base is a feasible binding mode (*15*). We also demonstrated that the G-N7 monoadduct is thermally stable and does not transform into cross-links promoted by the loss of ACRAMTU or en ligands (*15*). Here, we present the NMR-derived structure of the guanine-N7 adduct in a site-specifically modified octamer, d(5′-CCTCG*TCC-3′/5′-GGACGAGG-3′) (**III***, Chart 1), where the asterisk indicates the [Pt(en)(ACRAMTU)]$^{3+}$ ($PtN_2S$) fragment. The current study reports the first solution structure of a DNA adduct formed by a bioactive platinum−intercalator conjugate. Critical differences between this adduct and the common 1,2-intrastrand cross-link emerge, which may ultimately lead to damage recognition by proteins and DNA-processing enzymes dissimilar to that of the adducts formed by the clinical agent cisplatin.

## MATERIALS AND METHODS

*Starting Materials*. The synthesis and characterization of PT-ACRAMTU was published earlier (*7*). PT-ACRAMTU was used as its nitrate salt. Buffers were made from biochemical grade chemicals (Fisher/Acros) using 0.22 $\mu$m-filtered DNase/RNase-free water obtained from a Milli-Q A10 synthesis water purification system. All experiments were carried out in a buffer containing 10 mM sodium phosphate and 10 mM NaCl (pH 7.3). HPLC-grade solvents were used for all chromatographic separations. All other chemicals and reagents were purchased from common vendors and used without further purification. The oligodeoxyribonucleotides 5′-CCTCGTCC-3′ (sequence **I**) and 5′-GGACGAGG-3′ (sequence **II**) were purchased from Integrated DNA Technologies Inc. (Coralville, IA). The sequences were synthesized using phosphoramidite chemistry and desalted by the vendor. The DNA strands were quantified by UV−visible spectroscopy using the molar extinction coefficients $\epsilon_{I,260}$ = 63 700 L/cm mol and $\epsilon_{II,260}$ = 85 100 L/cm mol provided by the vendor. Solutions of the DNA−drug adduct were stored at −20 °C.

*Synthesis and Purification of the Platinum-Modified Top Strand (**I***)*. Sequence **I** (17.5 $\mu$mol) was incubated with 1.1 equiv (19.3 $\mu$mol) of PT-ACRAMTU in 4 mL of water (pH 6.0) at 37 °C in the dark for 5 days. The reaction was followed by HPLC (LaChrom Hitachi D-7000 system equipped with an L-7420 UV−visible variable-wavelength detector). A semipreparative reverse-phase column (250 × 9.4 mm; Agilent, Zorbax SB−C18) was used for both monitoring the progress of the reaction and product isolation. Chromatograms were recorded at wavelengths of 254 and

413 nm for analytical purposes and at 285 nm during adduct collection. The separation of the reaction mixture was carried out using the following conditions: mobile phase, solvent A = 100 mM ammonium acetate, pH 7.0; solvent B = 100% acetonitrile; gradient: 90% A/10% B → 80% A/20% B over a period of 40 min at a flow rate of 3 mL/min. The platinated strand, **I***, was collected, lyophilized, redissolved in 1 mL of water, and desalted by exhaustive dialysis against deionized water (Spectrum Spectro/Por CE membrane, 1000 Da molecular weight cutoff). MALDI-TOF mass spectra of a desalted sample of **I*** were recorded on a Voyager DE instrument (Applied Biosystems Inc., Foster City, CA) by HT-Laboratories (San Diego, CA).

*Duplex Preparation.* The unmodified and modified duplexes **III** and **III*** were generated by mixing suitable aliquots of buffered solutions of **II** with **I** and **I***, respectively. To ensure complete double-strand formation, the samples were annealed by heating at 75 °C for 2 min and slow cooling to room temperature. Concentrations of the strands were determined spectrophotometrically using the molar extinction coefficients $\epsilon_{260}$ for the oligonucleotides (vide supra) and $\epsilon_{420} = 6.44 \times 10^3$ L/cm mol for DNA-bound acridine (*10*). Stoichiometic duplex formation was established using continuous variation titrations (Job plot analysis) (*16*) and titrations of **I*** with **II** in the NMR tube. The following numbering scheme was used for **III** and **III***:

```
5′-C(1) C(2) T(3) C(4) G(*)(5)T(6) C(7) C(8)-3′
3′-G(16)G(15)A(14)G(13)C(12) A(11)G(10)G(9)-5′
```

The phosphodiester linkages (not shown) are numbered 5′ → 3′ starting with P2 in the top strand and P10 in the bottom strand.

*Circular Dichroism Spectropolarimetry*. CD experiments were performed on an AVIV model 215 spectrophotometer equipped with a thermoelectrically controlled cell holder. Quartz cells with 1-cm path length were used for all experiments. Before data collection, samples were annealed by slow cooling from 75 °C to room temperature. The concentrations of modified duplex (**III***) were 3.5 and 73 $\mu$M for CD spectra recorded in the UV (200−325 nm) and UV−visible (320−600 nm) regions, respectively. Isothermal CD spectra at 25 °C were recorded in 1-nm increments with an averaging time of 1 s.

*Optical Studies of Thermal Denaturation*. The melting profiles were recorded on a HP 8453 diode array spectrophotometer equipped with a Peltier temperature-controlled cell holder unit and an external temperature probe. Quartz cells with 1-cm path length were used in all experiments. Concentrations of **III** and **III*** were 2.2 and 3.7 $\mu$M, respectively. Absorbance as a function of temperature was measured at 260 nm. The temperature was changed in 1 °C increments from 10 to 70 °C and back to 10 °C, and the stirred samples were allowed to equilibrate for 2 min at each temperature setting. Absorbance data were fitted to the baseline-corrected two-state helix-coil transition model (*17*). Melting temperatures ($T_m$) were extracted directly from the curve fits. Thermal melting experiments for each duplex were performed in triplicate. Analysis of the melting transitions was carried out using the custom-defined nonlinear fitting option of Microcal Origin 6.0 (OriginLab Corp., Northampton, MA).

*NMR Spectroscopy*. Duplexes **III** and **III*** were dissolved in 300 $\mu$L of phosphate buffer (10 mM $Na_2HPO_4$, 10 mM NaCl, pH* 7.0), lyophilized to dryness, and relyophilized twice from 99.96% $D_2O$. NMR samples were made by dissolving the duplexes in 300 $\mu$L of 99.996% $D_2O$ to afford a concentration of approximately 3.5−4 mM in double-stranded oligonucleotide. For exchangeable proton NMR spectra, the samples were dissolved in 90% $H_2O$/10% $D_2O$. A Shigemi NMR microtube (Shigemi Inc., Allison Park, PA) was used for data collection. $^1$H NMR spectra were acquired at 500 MHz on a Bruker DRX-500 spectrometer equipped with a 5-mm inverse 3-channel Z-gradient TBI probe. All $^1$H 1-D and $^1$H−$^1$H 2-D NMR spectra were acquired at 25 °C with a spectral width of either 4500 Hz (nonexchangeable proton spectra) or 11000 Hz (exchangeable proton spectra) with the carrier frequency set to the HDO signal. Proton chemical shifts were referenced to the HDO peak, which was calibrated against external 3-(trimethylsilyl)-1-propanesulfonic acid sodium salt (DSS). $^{31}$P chemical shifts were referenced relative to an external 85% phosphoric acid sample.

1-D $^1$H NMR spectra were recorded with a total of 64 k data points, 128 transients, and a recycle delay of 1 s. The water suppression by gradient-tailored excitation (WATERGATE) or double pulsed field gradient spin−echo (DPFGSE) techniques (*18*) or presaturation pulses were used to suppress the HDO peak. The time domain data were apodized with an exponential window function using a line broadening of 0.3−1.0 Hz before Fourier transformation. Spectra were processed using the XWinNMR 2.6 software (Bruker, Ettlingen, Germany). Homonuclear $^1$H−$^1$H and heteronuclear $^1$H−$^{31}$P NMR data sets (for both **III** and **III***) were acquired with 2048 complex points in $t_2$, 512 points in $t_1$, and 64 transients with a recycle delay of 2 s, except for the dqf-COSY (double quantum-filtered correlation spectroscopy) data, which were collected with 2048 complex points in $t_2$, 1024 points in $t_1$, and 64 transients per $t_1$ increment. The $^1$H-detected $^1$H−$^{31}$P correlated spectra ($^1$H−$^{31}$P dqf-COSY) were acquired with a spectral width of 3000 Hz in $t_2$ ($^1$H) and 3650 Hz in $t_1$ ($^{31}$P). A spin-lock time of 80 ms was used in all total correlation spectroscopy (TOCSY) experiments. Nuclear Overhauser enhancement spectroscopy (2-D NOESY) spectra were acquired with mixing times ($\tau_m$) of 150, 250, and 350 ms. For exchangeable protons, a NOESY dataset was acquired with a mixing time of 350 ms in 90% $H_2O$/10% $D_2O$. All data were multiplied with optimized phase-shifted squared sinebell apodization functions and zero-filled to 2048 × 2048 data points before Fourier transformation. 2-D data sets were processed with Felix 2000 (Accelrys Inc., San Diego, CA) installed on a Silicon Graphics O2 workstation.

*2-D NOE Intensity Analysis and Distance Restraints*. NOE cross-peaks volumes were integrated using the program Felix 2000 (Accelrys Inc., San Diego, CA). For the initial refinement stage, interproton NOE distances were calculated from cross-peak volumes extracted from the NOESY spectrum acquired with a mixing time of 150 ms. NOE intensities were calibrated against an average intensity of the H5−H6 (2.45 Å) cross-peaks of the cytosine bases. The resulting distances were categorized as strong, medium, and weak, with boundaries of 1.8−3.0, 2.5−3.7, and 3.5−5.0 Å, respectively. For further structural refinement, NOESY

spectra acquired with 150 and 250 ms mixing times were analyzed by complete relaxation matrix calculations using the program MARDIGRAS (version 3.2; T. L. James; Department of Pharmaceutical Chemistry, University of California, San Francisco, CA). Only distances between nonexchangeable protons were generated. To account for peak integration errors due to signal overlap, each of the two intensity sets were assigned an error of 10%. The thymine and ACRAMTU methyl protons were treated with the three-site jump model. All MARDIGRAS calculations were carried out assuming a single isotropic correlation time of 2.25 ns. 164 intra-DNA and 15 drug−DNA NOE cross-peak intensities were used to calculate distance restraints. Using the RANDMARDI option of MARDIGRAS, a total of 30 runs were carried out for each experimental intensity data set. The resulting distance estimates from the two different mixing times were then averaged to give the final distance restraint file. The upper and lower bounds in this final distance restraint file were average distances ± 1 standard deviation. NOE-based distance restraints for contacts involving exchangeable protons were included in the early refinement stage only using a generous boundary of 1.5−5.0 Å.

*Calculation of the Structure of the Platinated Duplex (**III***)*. Calculations were performed using the program InsightII/Discover (release 2000, Molecular Simulations Inc., San Diego, CA). The AMBER force field (*19*) (version 1.6) was used in all molecular mechanics calculations. Gasteiger-Hückel partial charges for ACRAMTU were adopted from a previous study (*15*). The +2 charge on the platinum atom was distributed to the neighboring atoms according to a published scheme (*20*). New force constants, bond lengths, angles, and torsionals, partly based on existing AMBER parameters (*21*−*23*) were added to the existing parameter set and optimized to accurately reproduce key structural features in the crystal structure of the mononucleoside adduct, [Pt(en)ACRAMTU(dGuo-*N7*)]$^{3+}$ (dGuo*) (*14*). New atom types and parameters have been submitted as Supporting Information (Tables S3 and S4). A starting model of duplex **III*** was generated by truncating and mutating several DNA bases of a previously published AMBER model of a PT-ACRAMTU-modified B-form dodecamer (*15*). Solvent was simulated with a distance-dependent dielectric ($\epsilon = 4r_{ij}$). A cutoff of 20 Å was used for nonbonded interactions with a switching distance of 1.5 Å. Coulombic and 1-4 nonbonded interactions were scaled by a factor of 0.5. For all molecular dynamics calculations, a flat-bottomed potential was applied with an energy penalty of 200 kcal mol$^{-1}$ Å$^{-2}$. Inside the restraint boundaries, no energy penalty was applied. Additional distance restraints (100 kcal mol$^{-1}$ Å$^{-2}$) were introduced between Watson−Crick hydrogen-bonded donor-acceptor pairs (2.8−3.1 Å) in all molecular dynamics calculations. The starting structure was subjected to steepest descent and conjugate gradient minimization until the convergence criteria of $\Delta$rms = 0.01 kcal mol$^{-1}$ Å$^{-1}$ was satisfied. Strong, medium, and weak (1.8−3.0, 2.5−3.7, and 3.0−5.0 Å) NOE-based restraints were used for the initial restrained molecular dynamics/simulated annealing cycles. The preminimized structure was heated from 0 to 400 K over a period of 2.5 ps using a step size of 0.5 fs. Along the dynamics trajectory of 1.3 ns, snapshots of the structure were saved every 6.5 ps (4 ps of heating at 400 K and cooling to 150 K within 2.5 ps). The 200 structures generated along the trajectory were subjected to conjugate gradient minimization to a final rms derivative of 0.01 kcal mol$^{-1}$ Å$^{-1}$. A family of 20 low energy structures was identified from which an average structure was generated using the Analysis module in InsightII. This average structure was used as the starting structure for MARDIGRAS calculations. Several cycles of molecular dynamics/simulated annealing using distance bounds derived from MARDIGRAS calculations were performed until no significant NOE distance violations (>0.25 Å) were observed. Finally the structure was heated from 0 to 400 K over a period of 5 ps using a step size of 1 fs. Along the 0.5 ns dynamics trajectory, structures were saved every 10 ps (heating at 400 K for 7.5 ps and cooling to 150 K in 2.5 ps). Fifty structures were generated along the trajectory, which were initially minimized with restraints "on" and then with restraints "off" using steepest decent followed by conjugate gradient minimization to a maximum rms derivative of 0.01 kcal mol$^{-1}$ Å$^{-1}$. An ensemble of 19 low-energy structures was identified along the dynamics trajectory using cluster graphs generated with the Analysis module in InsightII from which an averaged structure was generated and minimized.

The program CORMA (version 5.2; T. L. James; Department of Pharmaceutical Chemistry, University of California, San Francisco, CA) was used to back-calculate the theoretical NMR intensities for the averaged structure. The $R^x$ sixth-root residual index (*24*), defined as $R^x = \sum|(a_o)_i^{1/6} - (a_c)_i^{1/6}|/\sum|(a_o)_i^{1/6}|$, was used to compare observed NOE intensities ($a_o$) with the calculated NOE intensities ($a_c$) based on the final ensemble of coordinates. $R^x$ was also calculated for the coordinates of the energy-minimized starting structure and the structure generated with Discover before the full-relaxation matrix analysis. Helical parameters were analyzed with NAMOT (version 2.1; G. Carter, C. S. Tung; Los Alamos National Laboratory, Los Alamos, NM). Plots were generated from pdb files using the DS Viewer Pro software (version 5.0; Accelrys Inc., San Diego, CA).

## RESULTS

*Preparation and Physical Characterization of the Modified and Unmodified Duplexes.* A duplex was designed containing a central 5′-(CG)$_2$ step and a single guanine base in the top strand, d(5′-CCTCGTCC-3′) (**I**), following a strategy described previously for a site-specifically modified dodecamer (*15*). Briefly, strand **I** was incubated with PT-ACRAMTU, and the resulting modified sequence (**I***) was purified by semipreparative HPLC and its structure confirmed by MALDI-TOF mass spectrometry. The mass spectrum recorded in positive-ion mode shows the expected peak for the singly charged [**I*** + 5H]$^+$ ion at *m*/*z* 2903, as well as minor fragment ions resulting from collision-induced loss of ACRAMTU (*m*/*z* 2568) and [Pt(en)ACRAMTU] (*m*/*z* 2326) (data not shown). To generate the model duplex, sequence **I*** was annealed to its complement, d(5′-GGAC-GAGG-3′) (**II**), giving the modified duplex **III*** (Chart 1). The analogous unmodified duplex, **III**, was also prepared (see Materials and Methods for details). Thermal melting curves (Figure 1a) were recorded for **III** and **III***, which indicate that both sequences exist in their double-stranded forms under the conditions of the NMR data acquisitions. The platinum adduct in **III*** increases the thermal stability

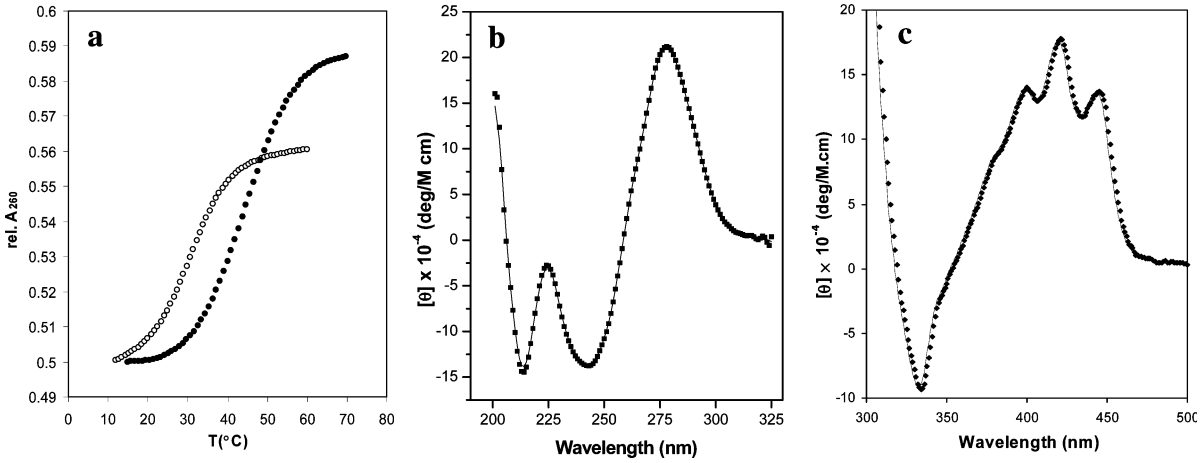


FIGURE 1: (a) Thermal melting curves recorded of duplexes **III** (open circles) and **III*** (solid circles). The melting temperatures (extracted from nonlinear curve fits) were $T_m$(**III**) = 31.7 °C and $T_m$(**III***) = 44.9 °C. (b) DNA region of the CD spectrum recorded at 25 °C of duplex **III***. (c) Induced circular dichroism (ICD) in **III*** in the acridine region of the CD spectrum. The band at 332 nm showing a negative sign is assigned to a $\pi-\pi^*$ transition polarized along the long axis of the aromatic system. The short-axis $\pi-\pi^*$ transition centered at $\lambda_{max}$ = 419 nm mimics the absorption spectrum of the acridine chromophore (see ref *15*). Experiments were performed in 10 mM sodium phosphate buffer containing 10 mM NaCl (pH 7.3).

of the host duplex by $\Delta T_m$ = 13.2 °C, consistent with earlier findings for similar modified oligonucleotides (*15*). (The thermodynamic implications of the melting behavior of the guanine-N7 adduct have been discussed in detail elsewhere (*15*).) CD spectra recorded for **III*** in the DNA region (200−325 nm; see Figure 1b) show a negative band at 241 nm and a positive band at 277 nm, which are the characteristic features of right-handed B-form DNA (*25*). Both bands appear red-shifted by 6 and 2 nm, respectively, compared to the CD signal of unmodified **III** (not shown). The distinct negative band at 213 nm, however, indicates a nonstandard B-form possessing A-type features (*26*). Figure 1c shows the characteristic induced circular dichroism (ICD) signal for the acridine chromophore, which results from insertion of the intrinsically achiral ligand into the DNA base stack (*15*).

*NMR Assignments*. Sequential assignments of exchangeable and nonexchangeable proton resonances were based on TOCSY, NOESY, and dqf-COSY spectral data following standard literature procedures (*27*). Assignments were made using sequential NOE connectivities detected in NOESY spectra acquired with mixing times of $\tau_m$ = 350 ms in $D_2O$ or 90% $H_2O$/10% $D_2O$. Both H1′($i-1$) → H8/H6($i$) sequential contacts (shown in Figure S1, Supporting Information, for the top and bottom strand of duplexes **III** and **III***) and H3′($i-1$) → H8/H6($i$) interresidue connectivities (Figure 2) were used to unambiguously assign the base and deoxyribose protons. The adenine H2 protons were assigned from connectivities with the imino protons of complementary thymine in NOESY spectra of **III** and **III*** recorded in 90% $H_2O$/10% $D_2O$. The stereospecific assignment of the H2′ and H2″ protons was made on the basis of H2′/H2″-H1′ NOE cross-peak intensities. Drug protons were assigned using NOESY and COSY spectra. $^{31}P$ chemical shifts were assigned via $^3J_{H3'-P}$ scalar couplings using proton-detected heteronuclear $^1H-^{31}P$ dqf-COSY experiments. Complete assignments including chemical shift differences ($\Delta\delta$) between duplexes **III** and **III*** have been deposited as Supporting Information in Tables S1 and S2.

*NMR Spectral Changes Caused by the Guanine-N7 Adduct*. In the 1-D and 2-D NMR spectra of the modified

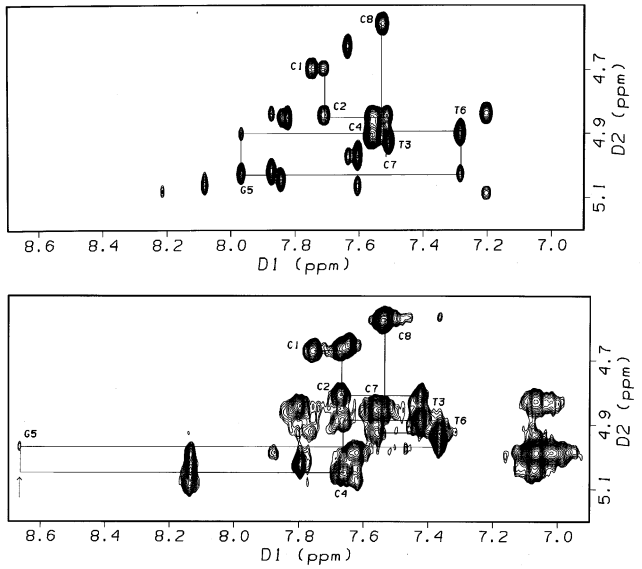


FIGURE 2: Sections of the 2-D NOESY spectra (500 MHz, 298 K, $D_2O$, pH* 7.0, $\tau_m$ = 350 ms) of duplexes **III** (top) and **III*** (bottom) showing sequential NOE connectivities for H3′($i-1$) → H8/H6($i$) in the top strands of the two sequences. Note the disruption of connectivity for C4H3′/G5*H8 and the low intensity of the intraresidue cross-peak for G5*H8/G5*H3′ (see text).

duplex **III***, H8 of the platinated nucleobase G5* was easily identified in the aromatic region as it experiences a characteristic downfield shift of $\Delta\delta$ 0.704 ppm as a consequence of platinum binding to the endocyclic N7 position of the base (*28*). A critical observation made during the assignment of the nonexchangeable protons in **III*** was the absence of several NOE connectivities both in the top and bottom strands at the 5′-C4G5*/C12G13 base-pair step. Figure 2 shows the expected connectivities for the top strands in **III** and **III***. While the sequential "NOE walk" was uninterrupted for **III**, the NOE cross-peak between C4H3′ and G5H8 is clearly absent for the modified strand of **III***. Interruption of the connectivity pattern in the top and bottom strands at the adduct site was also found in the H1′/H8/H6 region of the NOESY spectrum of **III*** (Figure S1, Supporting Information). This is in contrast to complexes of reversible ACRA-

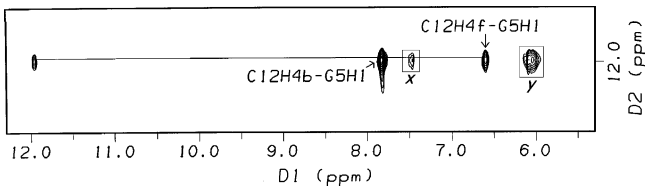


FIGURE 3: Expanded section of the 2-D NOESY spectrum (500 MHz, 298 K, 90% $H_2O$/10% $D_2O$, pH* 7.0) of duplex **III*** with cross-peaks resulting from interstrand base−base contacts labeled. H4b is the cytosine amino proton involved in Watson−Crick hydrogen bonding; H4f is the proton not involved in hydrogen bonding. The boxed cross-peaks labeled *x* and *y* result from NOE contacts between the G5* imino proton and H5 and H6 of the intercalated acridine chromophore.

MTU, where rapid on/off rates and delocalization of the intercalator over multiple sites did not significantly reduce internucleotide cross-peak intensities along the "NOE walk" (*12*). The perturbations observed for **III*** at the early stages of the NMR investigation indicated conformational changes in the octanucleotide compatible with intercalation of acridine on the 5′ face of the modified nucleobase. While the missing cross-peaks are consistent with distortions along the helical axis, strong cross-peaks were detected between the exchangeable imino proton G5*H1 and the exocyclic $NH_2$ protons C12H4b/C12H4f on the opposite strand (Figure 3), indicating that Watson−Crick hydrogen bonding persists between platinated guanine and complementary cytosine.

In addition to the distinct downfield shift of G5H8 upon platination, chemical shift perturbations are observed that support the regioselective intercalation of the platinum-tethered ACRAMTU ligand into the 5′-C4G5*/C12G13 base-pair step: As a result of the conformational changes and the ring current effect of the planar drug chromophore, several of the base and deoxyribose protons at this base step experience significant upfield or downfield shifts relative to the free oligonucleotide (summarized in Figure 4a). The resonances for the minor-groove H1′ protons on residues C4 and G5* of the platinated strand, for instance, are upfield shifted by 0.169 and 0.136 ppm, respectively. Conversely, H1′ resonances of the complementary bases, C12 and G13, are shifted downfield by 0.247 and 0.180 ppm, respectively. Shift changes of similar magnitude are also observed for the H2′ and H2″ resonances at this base-pair step. The most pronounced effect, however, is observed for the guanine imino protons: upfield shifts of 0.841 for G5*H1 and 1.193 ppm for G13H1 are consistent with a large local shielding effect caused by the intercalated acridine ring system (*29*). Likewise, characteristic shift changes are observed within the $[Pt(en)ACRAMTU]^{3+}$ fragment in **III*** relative to the resonances of unbound PT-ACRAMTU (Figure 4b): A common spectral feature was the pronounced upfield shifts of 0.226−1.388 ppm of the H1−H8 signals of the acridine moiety indicating intercalative binding of the planar ring. The methylene H11 and H12 protons in the linker chain are affected in the same way. In contrast, the methyl protons H13 and H14 show the opposite effect, resulting in a significant downfield shift of 0.503 and 0.350 ppm, respectively. The chemical shift changes observed for an intercalated chromophore are dominated by aromatic ring current effects of the sandwiched nucleobases and depend on the relative positioning of the drug with respect to the duplex. The $\Delta\delta$ values are in accordance with previously reported data for DNA complexes of ACRAMTU (*10*, *12*). The magnitude and sign of the shifts suggest that the H1−H12 containing portion of ACRAMTU penetrates the base stack, while the thiourea methyl groups lie in the DNA groove where they experience the deshielding ring current effects of the base-pair edges.

$^{31}P$ chemical shifts have been demonstrated to be linearly correlated with local DNA helix unwinding angles (*30*): intercalating agents cause a decrease in the helical twist of the modified duplex compared to standard B-form DNA resulting in a deshielding of the $^{31}P$ nuclei at the binding site. $^1H-^{31}P$ correlated spectra were recorded of duplexes **III** and **III*** (Figure 5a,b), from which $\Delta\delta(^{31}P)$ values were extracted (Figure 5c). The most pronounced shift perturbations are observed for phosphate residues P5 and P13 at the central 5′-C4G5*/C12G13 base-pair step. The downfield shifts of the corresponding $^{31}P$ resonances of 1.160 and 0.462 ppm, respectively, are consistent with local backbone conformational changes resulting from the regioselective intercalation of ACRAMTU. On the basis of the $\Delta\delta(^{31}P)$ values, the backbone conformation at the base steps adjacent to the intercalation site is also affected, but to a lesser extent.

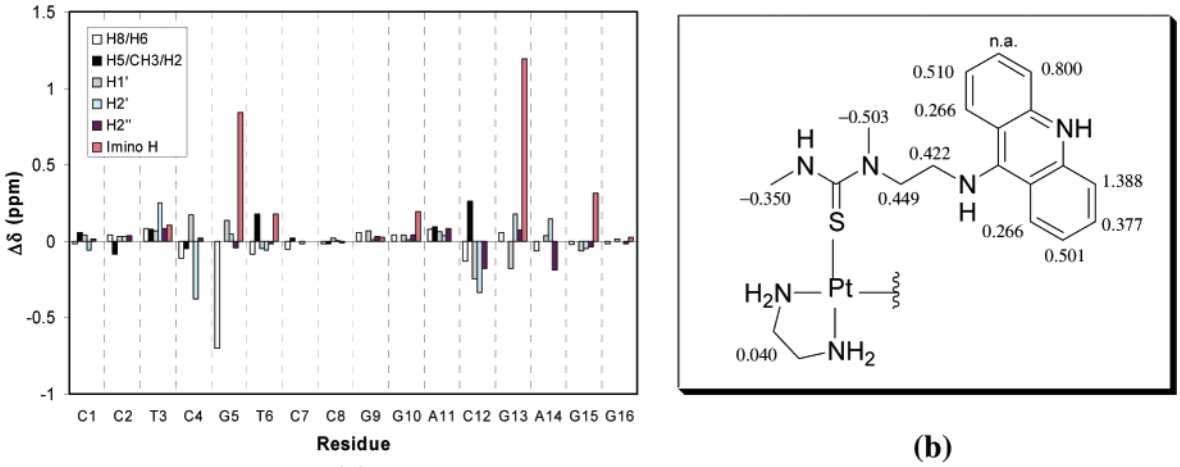


FIGURE 4: (a) Chemical shift changes ($\Delta\delta = \delta_{III} - \delta_{III*}$) for selected base and deoxyribose protons and (b) upfield (*positive sign*) and downfield (*negative sign*) shifts in the $[Pt(en)ACRAMTU]^{3+}$ fragment in duplex **III*** relative to the resonances in free PT-ACRAMTU (n.a. = not assigned due to peak overlap).

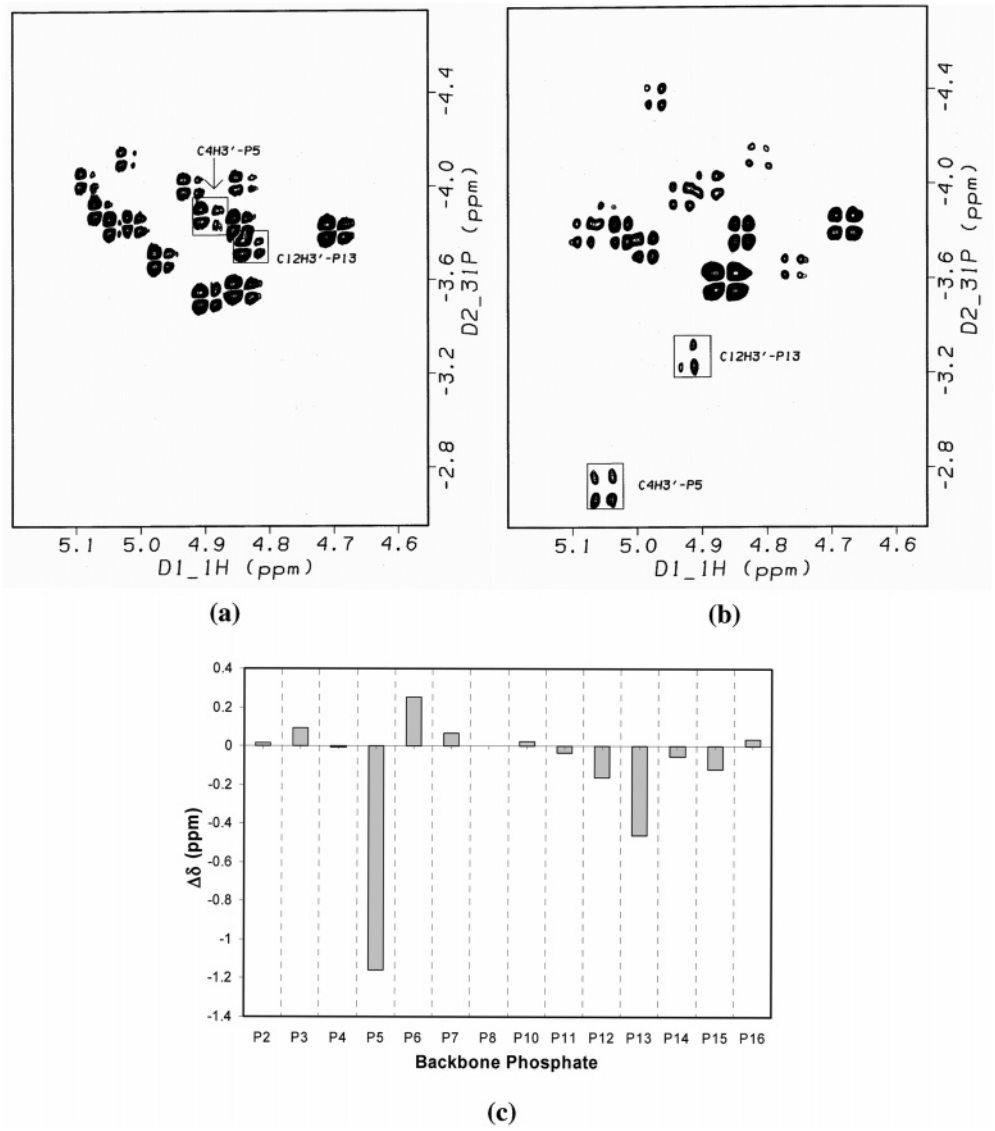


FIGURE 5: Sections of the $^{1}H-^{31}P$ dqf-COSY spectra ($D_2O$, pH* 7.0, 298 K) of the unmodified (a) and modified (b) duplexes **III** and **III*** showing scalar H3′-phosphorus connectivities. Cross-peaks assigned to the phosphate residues at the intercalation site (P5, P13) are boxed and labeled. Complete assignments are given in Table S1, Supporting Information. (c) Summary of $^{31}P$ chemical shift changes ($\Delta\delta = \delta_{\mathbf{III}} - \delta_{\mathbf{III*}}$) for the backbone phosphate residues.

Drug binding also causes changes in the deoxyribose conformations of G5* and the neighboring residues, C4 and T6. *J*-coupling analysis according to Rinkel and Altona (*31*) of $^{1}H-^{1}H$ COSY spectra showed that the conformation of the oligonucleotide in duplex **III*** deviates from the characteristic parameters of B-form DNA. The sums of vicinal couplings, ∑H1′, involving C4H1′ (13.2 Hz), G5*H1′ (15.4 Hz), and T6H1′ (13.2 Hz), while in accord with an *S*-type conformation for modified G5*, suggest that the adjacent residues have considerable *N*-type character (approximately 50% C3′-*endo*, assuming a dynamic model with rapid interconversion of the sugar puckers). For residues C12 and G13 on the opposite strand, no coupling information was extractable from the COSY data due to spectral overlap, and ∑A11H1′ was found to be 15.3 Hz. (For comparison, ∑H1′ values for all nonterminal residues of the unmodified duplex **III** were in the range 14.8−15.4 Hz, indicating predominant *S*-type character for all sugar residues in this sequence.) The weak NOE for G5H8-G5H3′ observed in NOESY spectra of **III*** taken with mixing times of 150, 250, and 350 ms is consistent with the *S*-type sugar pucker of the platinated residue deduced from the COSY data. The fact that this NOE is considerably weaker compared to that in the unmodified sequence **III** (Figure 2) may also point to an altered glycosidic torsion angle of G5* enforced by the bulky adduct. Similarly, the intensities of the H6/H8−H3′ intranucleotide NOE cross-peaks of all residues in duplex **III*** were classified as medium or weak, further corroborating that none of the sugar residues affected by the drug adopts a classical *C*3′-endo conformation (see stacked plot of the relevant NOESY section in Figure S2, Supporting Information).

*Drug−DNA Contacts*. A total of 20 well-resolved cross-peaks were observed in the NOESY spectra of duplex **III*** resulting from NOEs between ACRAMTU protons and protons at the 5′-C4G5*/C12G13 base-pair step of the oligonucleotide. (Fifteen of these NOEs involved non-exchangeable protons, which were included in the calculations of distance restraints, vide infra.) No NOEs were observed beyond the central residues, confirming that intercalation of the ACRAMTU moiety occurs regioselec-

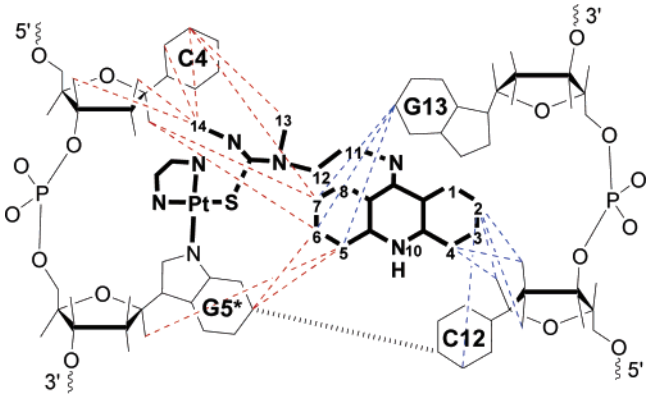


FIGURE 6: Summary of through-space connectivities detected in the 2-D NOESY spectra at all mixing times ($\tau_m$) of **III*** between exchangeable and nonexchangeable protons of the drug molecule and the oligodeoxyribonucleotide. Nuclear Overhauser effects involving the drug and the modified top strand and complementary bottom strand are indicated by red and blue dashed lines, respectively. (Several ambiguous NOEs involving the deoxyribose protons of G13 were not assigned due to spectral overlap.) The hashed line indicates NOE connectivities between imino and exocyclic amino protons of Watson−Crick base paired G5* and C12 (see Figure 3).

tively at the 5′-side of platinated G5. The pattern of intermolecular NOEs provides important details of the geometry of the adduct and the positioning of ACRAMTU relative to the duplex. Figure 6 summarizes the assigned through-space connectivities observed in the 2-D NOESY spectra. The edges of the planar chromophore make contacts with the top and bottom strand of the sequence, involving both base and deoxyribose protons of residues C4, G5*, C12, and G13. Several NOEs are observed between the two halves of the aromatic acridine moiety and major-groove and minor-groove protons (H1′, H2′, and H2″) at the edges of the base-pair pocket into which ACRAMTU intercalates. This suggests efficient penetration of the base stack by the aromatic ring system and an intercalation geometry in which the chromophore's long axis is aligned with the adjacent base pairs. Other crucial NOEs observed for the aromatic acridine protons to exchangeable and nonexchangeable nucleobase protons include G5*H1···ACRH5 and G5*H1···ACRH6 (Figure 3). The methyl protons of the thiourea linker (H13, H14) show NOEs to C4H5, C4H6, and C4H2′/H3′, demonstrating that the nonintercalating thiourea moiety of the drug lies in the major groove and is oriented toward the 5′-end of the modified strand, on the 5′-side of platinated G5.

*Computation of the 3-D Structure of the Modified Duplex, **III****.* A refined structure was generated for **III*** based on distance restraints calculated from 179 NOE intensities, including 15 resulting from contacts between the [Pt(en)-ACRAMTU]$^{3+}$ fragment and the oligonucleotide. The number of usable NOE intensities was limited due to spectral overlap in the 2-D NOESY spectra, and only high-quality cross-peaks were considered that could be accurately integrated. Torsional constraints were not used in this study. The structure of **III*** was generated using a newly parametrized AMBER force field and a combination of rMD/simulated annealing protocols followed by complete relaxation matrix analysis. A previously reported suitably modified and truncated AMBER model of a PT-ACRAMTU-modified B-form duplex was used as the starting structure (*15*). Briefly, at the initial stage of the calculations the NOE cross-peaks

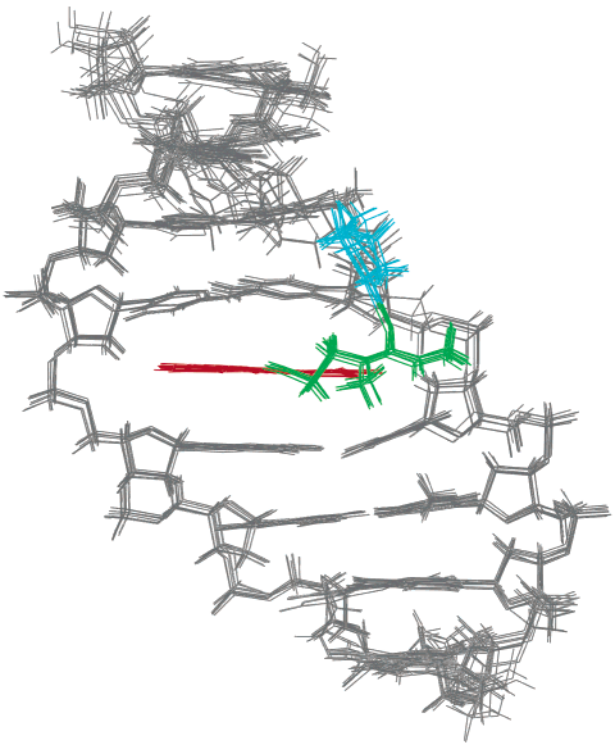

FIGURE 7: View of the 19 superimposed converged rMD structures of the modified duplex **III*** for which an average structure was calculated. The [Pt(en)]$^{2+}$ moiety, the thiourea linker chain, and the acridine chromophore are depicted in blue, green, and red, respectively.

were categorized as strong, medium, and weak and assigned appropriate distance bounds to produce a large number of rMD structures. From these, an energy-minimized average structure was generated, which was subjected to multiple cycles of iterative refinement using MARDIGRAS (see Materials and Methods for details). During the final refinement cycles, an ensemble of 19 structures of similar low energies was identified toward the end of the dynamics trajectory, which were considered converged based on pairwise RMSD values of less than 1.05 Å (Figure 7). An $r^6$ weighted *R*-factor ($R^x$) of $9.2 \times 10^{-2}$ was calculated using the program CORMA, indicating that this family of structures represented the experimental NOE intensities most accurately. For comparison, $R^x$ values of $1.35 \times 10^{-1}$ and $1.16 \times 10^{-1}$, respectively, were calculated for the minimized starting structure and the average rMD structure prior to the MARDIGRAS calculations. The high residual index for the starting structure can be, in part, explained with the discrepancy in measured and theoretical NOE intensities resulting from an incorrect alignment of the drug molecule with respect to the host duplex in the AMBER-derived structure. While our previous model (*15*) was able to correctly predict the regiospecificity of intercalation, the thiourea linker was located on the 3′-side of the platinated guanine base and not on the 5′-side, which was inconsistent with several crucial intermolecular NOEs detected in this study (see Figure 6). This problem was corrected during the early stage of the rMD simulations.

## DISCUSSION

Representative views of the final averaged and strain-minimized structure of **III*** calculated from the 19 rMD

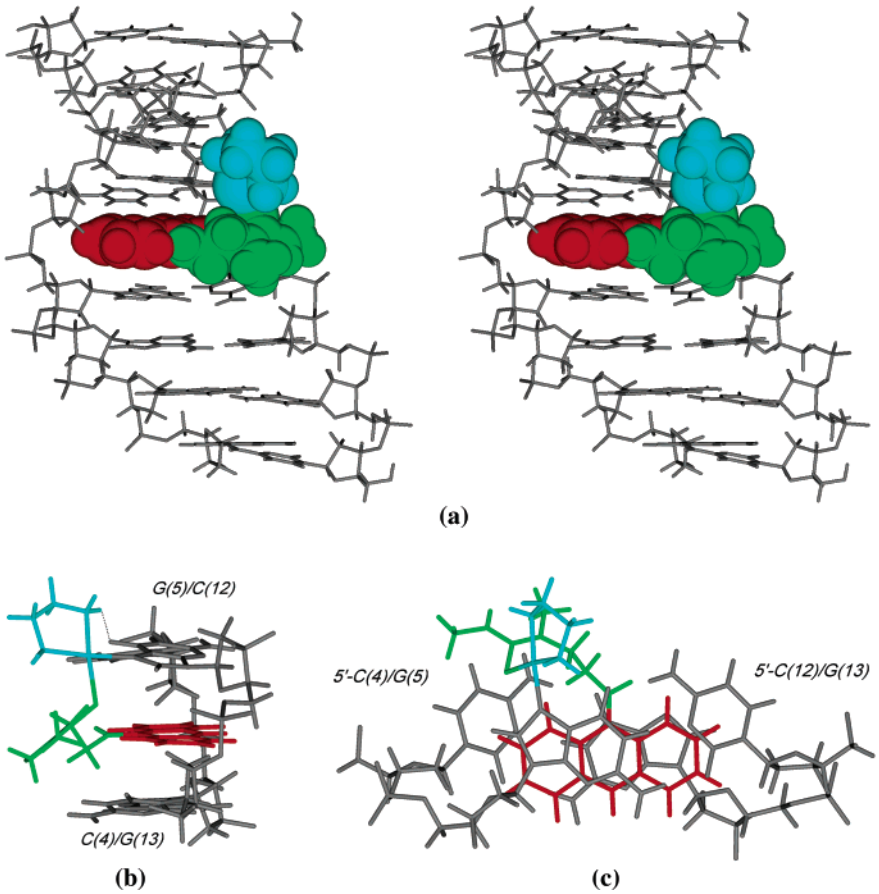


FIGURE 8: Final structure of duplex **III*** averaged from a family of 19 rMD structures and energy-minimized. (a) Stereoview into the major groove. The drug molecule is represented as van der Waals spheres. (b) Side view of the intercalation site and (c) view along the helical axis with DNA residues labeled. The dotted line in (b) indicates intermolecular hydrogen bonding (see text). The platinum moiety, thiourea linker, and acridine chromophore are depicted in blue, green, and red, respectively.

geometries are shown in Figure 8. The major groove of the host duplex accommodates the bulky monoadduct without disrupting the right-handed helix structure (Figure 8a), which is supported by the thermal melting and CD data. Watson−Crick hydrogen bonding is intact at the adduct site and throughout the duplex. At the site of platination, the planes through G5* and the square-planar platinum complex make a dihedral angle of ∼60°, which positions the en nonleaving group on the 3′-side and sulfur-linked ACRAMTU on the 5′-side of the modified nucleobase. This geometry allows regiospecific intercalation of the acridine chromophore into the 5′-C4G5*/C12G13 site. In the nonintercalating moiety of the drug, one of the en-$NH_2$ groups is involved in hydrogen bonding with exocyclic O6 of G5* ($N_{en}$···G5O6 2.91 Å), while the rest of the Pt moiety is directed out of the major groove. In contrast, the alkylated thiourea residue makes hydrophobic contacts with the wall of the major groove on the adduct side involving the base protons of the 5′-C4 residue (Figure 8b). The acridine moiety intercalates parallel to the adjacent base pairs, i.e., with the long axes of the drug chromophore and the adjacent base pairs adopting a collinear, rather than perpendicular, orientation (Figure 8c). This binding geometry, which maximizes $\pi-\pi$ stacking interactions between the drug and the DNA nucleobases, is commonly observed for acridines (*32*, *33*). In essence, the conjugate PT-ACRAMTU seems to be well designed to allow strainless dual binding involving major-groove N7 platination and a parallel intercalation mode coplanar with the DNA base stack. The crystal structure of the platinum-modified mononucleoside fragment dGuo* (Chart 1) indicated that combined platination of G-N7 and ideal coplanar stacking of acridine with adjacent base pairs is highly feasible (*14*). In dGuo*, acridine stacking stabilizes a rare type of $GG^-$ mispairing, probably because of increased $\pi$-stacking interactions with a *base pair* compared to a single base. We suggested that the distinct geometry observed in this model may have some relevance for the adducts formed by PT-ACRAMTU in double-stranded DNA (*14*). The superimposed structures of the $[Pt(en)ACRAMTU(guanine\text{-}N7)]^{3+}$ fragments in dGuo* and duplex **III*** (Figure S3, Supporting Information), indeed, demonstrate that the relative orientations of the bases and the folding pattern of the thiourea linker chains in both structures are very similar.

Characteristic perturbations of the duplex structure are observed at the drug binding site. Selected helical parameters for **III*** are summarized in Figure 9 (for additional parameters, see Figure S4 and Table S5, Supporting Information). Penetration of the DNA base stack by acridine causes a characteristic lengthening and unwinding of the duplex, as evidenced by a rise ($D_z$) of 6.62 Å and helical twist angle ($\Omega$) of 15.4° at the central base-pair step. Assuming a helical twist of 36° for regular B-form DNA (*34*), the latter value is in good agreement with the unwinding angle $\phi$ of 21°/adduct determined for PT-ACRAMTU in plasmid DNA using gel mobility shift assays (*10*). The regioselective intercalation of acridine into the 5′-CG*/CG base-pair step

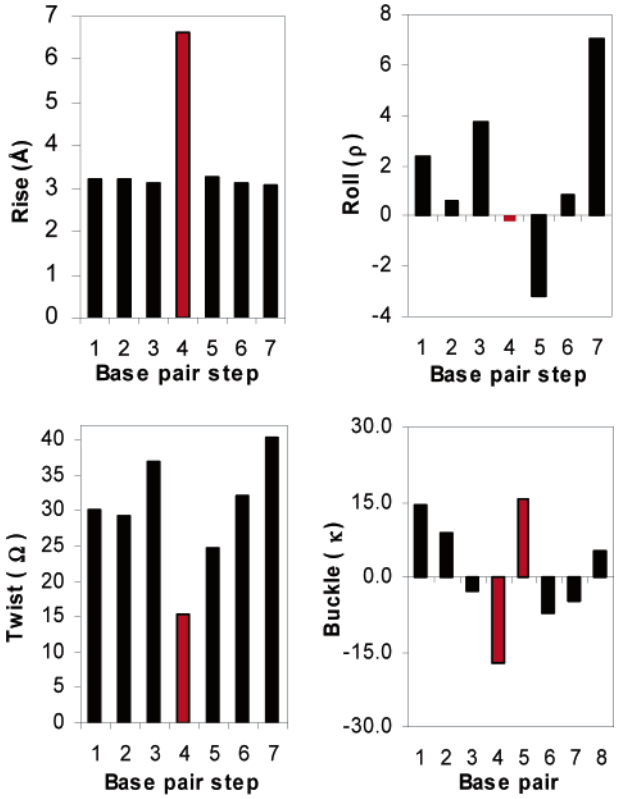


FIGURE 9: Selected base pair and base-pair step parameters calculated for the platinated duplex **III***. Columns representing values for the central 5′-C4G5*/C12G13 site are colored in red.

and the local DNA distortion associated with it provide a good explanation for the inhibition of T7 RNA polymerase observed in previous footprinting experiments (*13*). The enzyme, which acts on the modified template strand from the 3′- to the 5′-end, is unable to extend the newly synthesized strand past the intercalated chromophore, stalling transcription at 3′-G* sites. Also noticeable at the intercalation site is the buckling of the base pairs adjacent to the acridine chromophore: negative and positive buckles ($\kappa$) of −17.1° and 15.7° were calculated for C4G13 and G5*C12, respectively. Close inspection of the adduct site suggests that partial insertion into the base stack of the ethylene linker chain of ACRAMTU [$CH_2$(11)$CH_2$(12)] (supported by the upfield shifts of the corresponding proton resonances, vide supra) are responsible for this distortion. Both effects, the buckling and unwinding, explains the pronounced increase in van't Hoff entropy of the duplex upon drug binding (*15*). Another characteristic feature of the coordinative−intercalative adduct in **III*** is that the central base-pair step exhibits the smallest roll angle ($\rho = -0.2°$) in the entire sequence, suggesting that intercalated acridine enforces coplanarity between the adjacent C4G13 and G5*C12 base pairs.

The average pseudorotation angle (*P*) for the deoxyribose residues in **III*** is 94°, indicating that the duplex deviates significantly from typical B-form DNA. Eleven of the residues adopt an O4′-endo conformation ($P > 90°$, *S*-type), including G5*, which is 96°, while five are in the C4′-exo form ($P < 90°$, *N*-type). In addition, the glycosidic torsion angles ($\chi$) show significantly higher values than typically found in B-DNA (Table S5, Supporting Information) (*35*). Thus, duplex **III*** displays some features of A-form DNA. On the other hand, the groove dimensions and other helical parameters, such as the average roll angle (1.6°) and the average rise (3.6 Å), are reminiscent of B-DNA (*35*).

The most striking feature in the structure of duplex **III*** is that the oligonucleotide accommodates the adduct without apparent bending of the helix. This contrasts with the structural distortions produced by the bifunctional adducts formed by cisplatin and its analogues. The 1,2-intrastrand GG cross-link (*2*), for instance, is characterized by a directed bend of ∼30−40° toward the major groove, which is a consequence of the large roll angle between the platinated guanine bases. There is considerable variation in the reported bend angles determined from high-resolution NMR (*36*−*38*) and X-ray studies (*39*) and gel mobility shift assays (*40*). Considerable bending of the DNA helix has also been observed for the minor adducts of cisplatin [1,2-GG interstrand (*41*) and 1,3-GTG intrastrand (*42*) cross-links]. In the NMR solution structure of d(5′-CCTG*G*TCC-3′/5′-GGACCAGG-3′) modified with the 1,2-intrastrand cross-link, a sequence very similar to **III***, the sharp helical bend is associated with an inversion of the platinated 5′-G deoxyribose pucker from C2′-endo to C3′-endo (*37*). In this structure, the head-to-head orientation of the platinated guanine bases produces a strong NOE between G4*H8 and G5*H8. The kink positions G5*H8 beneath the adjacent G4* base, resulting in a considerably upfield shifted $^1$H NMR signal for this proton due to the shielding ring current effect of G4*. Analogous spectroscopic and structural features and the associated large roll angle at the platinum binding site are clearly absent at the 5′-C4G5*/C12G13 step in **III***. This difference in the geometric distortions produced by the coordinative−intercalative monoadduct and the GG intrastrand cross-link is also reflected in the macroscopic physical properties of the modified duplexes: PT-ACRAMTU causes a pronounced increase in thermal stability of the host duplex, whereas cisplatin shows the opposite effect (*43*). In this respect, PT-ACRAMTU also behaves differently from other "pseudobifunctional" platinum complexes bearing rigidly linked planar aromatic ligands, which destabilize DNA significantly (*44*) and cause cisplatin-type DNA structural distortions (*45*). The bending of cisplatin-modified DNA has been demonstrated to have profound consequences for DNA−protein recognition (*2*). HMG-domain proteins (*46*) and TATA binding protein (TBP) (*47*) recognize the damaged DNA and bind tightly to it through the widened minor groove at the site of platination, thereby interfering with the repair and transcription of the cell's DNA. Thus, these ternary complexes have been implicated as possible mediators or enhancers of cisplatin-induced apoptotic cancer cell death. On the basis of the NMR structure of duplex **III***, the dual coordinative−intercalative DNA binding mode of PT-ACRAMTU is not a mimic of the major cisplatin−DNA cross-link. As a consequence, PT-ACRAMTU may trigger apoptosis by a mechanism different from that of the clinical agent. Finally, it should be mentioned that among the DNA binders acting through a dual binding mechanism, several G-N7 alkylating−intercalating agents, such as the antitumor active natural products hedamycin and psorospermin (*48*−*50*), form DNA adducts intriguingly similar to the G-N7 adduct of PT-ACRAMTU. Further study of this analogy may give important hints about the potential mechanism of action of PT-ACRAMTU and assist the design of improved derivatives of this unusual hybrid drug.

## ACKNOWLEDGMENT

We thank Dr. Bernard A. Brown II for his help with formatting structural data for deposition with the Brookhaven Protein Data Bank.

## SUPPORTING INFORMATION AVAILABLE

Tables giving chemical shift assignments, AMBER parameters and fractional charges, and DNA structural parameters for the final minimized structure of the modified duplex **III***; figures of sections of the 350-ms NOESY spectra of the modified and unmodified duplexes showing sequential NOE connectivities and a stacked plot showing cross-peak intensities in the H8/H6-deoxyribose region, a stereoview of the superimposed G* fragments in duplex **III*** and in the crystal structure of dGuo*, and a graphical presentation of base pair and base-pair step parameters for **III***. This material is available free of charge via the Internet at http://www.pubs.acs.org.

## REFERENCES

1. Baruah, H., Barry, C. G., and Bierbach, U. (2004) Platinum-intercalator conjugates: from DNA-targeted cisplatin derivatives to adenine binding complexes as potential modulators of gene regulation, *Curr. Top. Med. Chem. 4*, 1537−1549.
2. Jamieson, E. R., and Lippard, S. J. (1999) Structure, recognition, and processing of cisplatin-DNA adducts, *Chem. Rev. 99*, 2467−2498.
3. Burstyn, J. N., Heiger-Bernays, W. J., Cohen, S. M., and Lippard, S. J. (2000) Formation of *cis*-diamminedichloroplatinum(II) 1,2-intrastrand cross-links on DNA is flanking-sequence independent, *Nucleic Acids Res. 28*, 4237−4243.
4. Hurley, L. H. (2002) DNA and its associated processes as targets for cancer therapy, *Nat. Rev. Cancer 2*, 188−200.
5. Kostrhunova, H., and Brabec, V. (2000) Conformational analysis of site-specific DNA cross-links of cisplatin-distamycin conjugates, *Biochemistry 39*, 12639−12649.
6. Loskotova, H., and Brabec, V. (1999) DNA interactions of cisplatin tethered to the DNA minor groove binder distamycin, *Eur. J. Biochem. 266*, 392−402.
7. Martins, E. T., Baruah, H., Kramarczyk, J., Saluta, G., Day, C. S., Kucera, G. L., and Bierbach, U. (2001) Design, synthesis, and biological activity of a novel non-cisplatin-type platinum-acridine pharmacophore, *J. Med. Chem. 44*, 4492−4496.
8. Hess, S. M., Anderson, J. G., and Bierbach, U. (2004) A non-crosslinking platinum-acridine hybrid agent shows enhanced cytotoxicity compared to clinical BCNU and cisplatin in glioblastoma cells, *Bioorg. Med. Chem. Lett. 15*, 443−446 (2005).
9. Hess, S. M., Mounce, A. M., Sequeira, R. C., Augustus, T. M., Ackley, M. C., and Bierbach, U. (2004) Platinum-acridinylthiourea conjugates show cell line specific cytotoxic enhancement in H460 lung carcinoma cells compared to cisplatin, *Cancer Chemother. Pharmacol*., in press.
10. Baruah, H., Rector, C. L., Monnier, S. M., and Bierbach, U. (2002) Mechanism of action of non-cisplatin type DNA-targeted platinum anticancer agents: DNA interactions of novel acridinylthioureas and their platinum conjugates, *Biochem. Pharmacol. 64*, 191−200.
11. Barry, C. G., Baruah, H., and Bierbach, U. (2003) Unprecedented monofunctional metalation of adenine nucleobase in guanine- and thymine-containing dinucleotide sequences by a cytotoxic platinum-acridine hybrid agent, *J. Am. Chem. Soc. 125*, 9629−9637.
12. Baruah, H., and Bierbach, U. (2003) Unusual intercalation of acridin-9-ylthiourea into the 5′-GA/TC DNA base step from the minor groove: implications for the covalent DNA adduct profile of a novel platinum-intercalator conjugate, *Nucleic Acids Res. 31*, 4138−4146.
13. Budiman, M. E., Alexander, R. W., and Bierbach, U. (2004) Unique base-step recognition by a platinum-acridinylthiourea conjugate leads to a DNA damage profile complementary to that of the anticancer drug cisplatin, *Biochemistry 43*, 8560−8567.
14. Baruah, H., Day, C. S., Wright, M. W., and Bierbach, U. (2004) Metal-intercalator-mediated self-association and one-dimensional aggregation in the structure of the excised major DNA adduct of a platinum-acridine agent, *J. Am. Chem. Soc. 126*, 4492−4493.
15. Baruah, H., and Bierbach, U. (2004) Biophysical characterization and molecular modeling of the coordinative-intercalative DNA monoadduct of a platinum-acridinylthiourea agent in a site-specifically modified dodecamer, *J. Biol. Inorg. Chem. 9*, 335−344.
16. Jenkins, T. C. Optical absorbance and fluorescence techniques for measuring DNA drug interactions, in *Drug DNA Interaction Protocols* (Fox, K. R., Ed.) pp 195−218, Totowa, Humana Press, 1997.
17. Marky, L. A., and Breslauer, K. J. (1987) Calculating thermodynamic data for transitions of any molecularity from equilibrium melting curves, *Biopolymers 26*, 1601−1620.
18. Braun, S., Kalinowski, H., and Berger, S. (1998) *150 and More Basic NMR Experiments*, pp 470−475, Wiley-VCH, Weinheim.
19. Weiner, S. J., Kollman, P. A., Case, D. A., Singh, U. C., Ghio, C., Alagona, G., Profeta, S., and Weiner, P. (1984) A new force-field for molecular mechanical simulation of nucleic-acids and proteins, *J. Am. Chem. Soc. 106*, 765−784.
20. Kozelka, J., Archer, S., Petsko, G. A., Lippard, S. J., and Quigley, G. J. (1987) Molecular mechanics modeling of oligonucleotide adducts of the antitumor drug *cis*-diamminedichloroplatinum(II), *Biopolymers 26*, 1245−1271.
21. Hambley, T. W. (1991) Molecular mechanics analysis of the stereochemical factors influencing monofunctional and bifunctional binding of *cis*-diamminedichloroplatinum(II) to adenine and guanine nucleobases in the sequences d(GpApGpG)·d(CpCpTpC) and d(GpGpApG)·d(CpTpCpC) of A- and B-DNA, *Inorg. Chem. 30*, 937−942.
22. Yao, S., Plastaras, J. P., and Marzilli, L. G. (1994) A Molecular mechanics AMBER-type force field for modeling platinum complexes of guanine derivatives, *Inorg. Chem. 33*, 6061−6077.
23. Bierbach, U., and Farrell, N. (1997) Modulation of nucleotide binding of trans platinum(II) complexes by planar ligands. A combined proton NMR and molecular mechanics study, *Inorg. Chem. 36*, 3657−3665.
24. Makley, J. L., Bax, A., Arata, Y., Hilbers, C. W., Kaptein, R., Sykes, B. D., Wright, P. E., and Wüthrich, K. (1998) Recommendations for the presentation of NMR structures of proteins and nucleic acids, *Pure Appl. Chem. 70*, 117−142.
25. Gray, D. M., Ratliff, R. L., and Vaughan, M. R. (1992) Circular dichroism spectroscopy of DNA, *Methods Enzymol. 211*, 389−406.
26. Vorlickova, M. (1995) Conformational transitions of alternating purine-pyrimidine DNAs in perchlorate ethanol solutions, *Biophys. J. 69*, 2033−2043.
27. Evans, J. N. S. *Biomolecular NMR Spectroscopy*, pp 343−391, Oxford University Press, New York, 1995.
28. Sletten, E., and Froystein, N. A. (1996) NMR studies of oligonucleotide-metal ion interactions, *Met. Ions Biol. Syst. 32*, 397−451.
29. Wilson, W. D., Li, Y., and Veal, J. M. (1992) NMR analysis of reversible nucleic acid small molecule complexes, in *Advances in DNA Sequence Specific Agents* (Hurley, L. H., Ed.) pp 89−165, JAI Press, New York.
30. Gorenstein, D. G., and Lai, K. (1989) $^{31}$P NMR spectra of ethidium, quinacrine, and daunomycin complexes with poly(adenylic acid-).poly(uridylic acid) RNA duplex and calf thymus DNA, *Biochemistry 28*, 2804−2812.
31. Rinkel, L. J., and Altona, C. (1987) Conformational analysis of the deoxyribofuranose ring in DNA by means of sums of proton−proton coupling constants: a graphical method, *J. Biomol. Struct. Dyn. 4*, 621−649.
32. Adams, A., Guss, J. M., Collyer, C. A., Denny, W. A., and Wakelin, L. P. G. (1999) Crystal structure of the topoisomerase II poison 9-amino-[N−(2-dimethylamino)ethyl]acridine-4-carboxamide bound to the DNA hexanucleotide d(CGTACG)$_2$, *Biochemistry 38*, 9221−9233.
33. Adams, A., Guss, J. M., Denny, W. A., and Wakelin, L. P. (2002) Crystal structure of 9-amino-N-[2-(4-morpholinyl)ethyl]-4-acridinecarboxamide bound to d(CGTACG)$_2$: implications for structure−activity relationships of acridinecarboxamide topoisomerase poisons, *Nucleic Acids Res. 30*, 719−725.
34. Neidle, S. (2002) *Nucleic Acid Structure and Recognition*, pp 31−61, Oxford University Press, New York.
35. Neidle, S. (2002) *Nucleic Acid Structure and Recognition*, pp 17−30, Oxford University Press, New York.

36. Gelasco, A., and Lippard, S. J. (1998) NMR solution structure of a DNA dodecamer duplex containing a *cis*-diammineplatinum-(II) d(GpG) intrastrand cross-link, the major adduct of the anticancer drug cisplatin, *Biochemistry 37*, 9230−9239.
37. Dunham, S. U., Dunham, S. U., Turner, C. J., and Lippard, S. J. (1998) Solution structure of a DNA duplex containing a nitroxide spin-labeled platinum d(GpG) intrastrand cross-link refined with NMR-derived long-range electron−proton distance restraints, *J. Am. Chem. Soc. 120*, 5395−5406.
38. Yang, D., van Boom, S. S. G. E., Reedijk, J., van Boom, J. H., and Wang, A. H.-J. (1995) Structure and isomerization of an intrastrand cisplatin-cross-linked octamer DNA duplex by NMR analysis, *Biochemistry 34*, 12912−12920.
39. Takahara, P. M., Frederick, C. A., and Lippard, S. J. (1996) Crystal structure of the anticancer drug cisplatin bound to duplex DNA, *J. Am. Chem. Soc. 118*, 12309−12321.
40. Bellon, S. F., and Lippard, S. J. (1990) Bending studies of DNA site-specifically modified by cisplatin, *trans*-diamminedichloroplatinum(II) and *cis*-[Pt($NH_3$)$_2$(N3-cytosine)Cl]$^+$, *Biophys. Chem. 35*, 179−188.
41. Huang, H., Zhu, L., Reid, B. R., Drobny, G. P., and Hopkins, P. B. (1995) Solution structure of a cisplatin-induced DNA interstrand cross-link, *Science 270*, 1842−1845.
42. Teuben, J. M., Bauer, C., Wang, A. H., and Reedijk, J. (1999) Solution structure of a DNA duplex containing a *cis*-diammineplatinum(II) 1,3-d(GTG) intrastrand cross-link, a major adduct in cells treated with the anticancer drug carboplatin, *Biochemistry 38*, 12305−12312.
43. Poklar, N., Pilch, D. S., Lippard, S. J., Redding, E. A., Dunham, S. U., and Breslauer, K. J. (1996) Influence of cisplatin intrastrand cross-linking on the conformation, thermal stability, and energetics of a 20-mer DNA duplex, *Proc. Natl. Acad. Sci. U.S.A. 93*, 7606−7611.
44. Bauer, C., Peleg-Shulman, T., Gibson, D., and Wang, A. H. (1998) Monofunctional platinum amine complexes destabilize DNA significantly, *Eur. J. Biochem. 256*, 253−260.
45. Kasparkova J., Novakova, O., Farrell, N., and Brabec V. (2003) DNA binding by antitumor *trans*-[$PtCl_2(NH_3)$(thiozole)]. Protein recognition and nucleotide excision repair of monofunctional adducts, *Biochemistry 42*, 792−800.
46. Cohen, S. M., Mikata, Y., He, Q., and Lippard, S. J. (2000) HMG-domain protein recognition of cisplatin 1,2-intrastrand d(GpG) cross-links in purine-rich sequence contexts, *Biochemistry 39*, 11771−11776.
47. Cohen, S. M., Jamieson, E. R., and Lippard, S. J. (2000) Enhanced binding of the TATA-binding protein to TATA boxes containing flanking cisplatin 1,2-cross-links, *Biochemistry 39*, 8259−8265.
48. Hansen, M., Lee, S.-J., Cassady, J. M., and Hurley, L. H. (1996) Molecular details of the structure of a psorospermin-DNA covalent/intercalation complex and associated DNA sequence selectivity, *J. Am. Chem. Soc. 118*, 5553−5561.
49. Hansen, M., Yun, S., and Hurley, L. (1995) Hedamycin intercalates the DNA helix and, through carbohydrate-mediated recognition in the minor groove, directs N7-alkylation of guanine in the major groove in a sequence-specific manner, *Chem. Biol. 2*, 229−240.
50. Owen, E. A., Burley, G. A., Carver, J. A., Wickham, G., and Keniry, M. A. (2002) Structural investigation of the hedamycin: d(ACCGGT)$_2$ complex by NMR and restrained molecular dynamics, *Biochem. Biophys. Res. Commun. 290*, 1602−1608.

BI050021B